Applied Physics Letters

Enhancing the piezoelectric modulus of wurtzite AlN by ion beam strain engineering

Cite as: Appl. Phys. Lett. **118**, 012108 (2021); https://doi.org/10.1063/5.0031047
Submitted: 29 September 2020 • Accepted: 16 December 2020 • Published Online: 07 January 2021

Holger Fiedler, Jérôme Leveneur, David R. G. Mitchell, et al.

COLLECTIONS

Paper published as part of the special topic on Ultrawide Bandgap Semiconductors

ARTICLES YOU MAY BE INTERESTED IN

AlScN: A III-V semiconductor based ferroelectric
Journal of Applied Physics **125**, 114103 (2019); https://doi.org/10.1063/1.5084945

Nitrogen-displacement-related electron traps in n-type GaN grown on a GaN freestanding substrate
Applied Physics Letters **118**, 012106 (2021); https://doi.org/10.1063/5.0035235

Effects of deposition conditions on the ferroelectric properties of ($Al_{1-x}Sc_x$)N thin films
Journal of Applied Physics **128**, 114103 (2020); https://doi.org/10.1063/5.0015281

© 2021 Author(s).

Applied Physics Letters ARTICLE scitation.org/journal/apl

Enhancing the piezoelectric modulus of wurtzite AlN by ion beam strain engineering

Cite as: Appl. Phys. Lett. **118**, 012108 (2021); doi: 10.1063/5.0031047
Submitted: 29 September 2020 · Accepted: 16 December 2020 ·
Published Online: 7 January 2021

View Online

Export Citation

CrossMark

Holger Fiedler,[1] Jérôme Leveneur,[1,2] David R. G. Mitchell,[3] Subramaniam Arulkumaran,[4,5] Geok Ing Ng,[4,6] Arokiaswami Alphones,[6] and John Kennedy[1,2,a)]

AFFILIATIONS

[1]National Isotope Centre, GNS Science, Lower Hutt 5010, New Zealand
[2]The MacDiarmid Institute for Advanced Materials and Nanotechnology, Wellington 6011, New Zealand
[3]Electron Microscopy Centre, Innovation Campus, University of Wollongong, Wollongong 2519, Australia
[4]Temasek Laboratories, Nanyang Technological University, Singapore 639798, Singapore
[5]Center for Integrated Research for Future Electronics (CIRFE), IMaSS, Nagoya University, Nagoya 464-8303, Japan
[6]School of Electrical and Electronics Engineering, Nanyang Technological University, Singapore 639798, Singapore

Note: This paper is part of the Special Topic on Ultrawide Bandgap Semiconductors.
[a)]**Author to whom correspondence should be addressed:** j.kennedy@gns.cri.nz

ABSTRACT

The piezoelectric modulus of wurtzite aluminum nitride (AlN) is a critical material parameter for electrical components, ultimately contributing to the energy efficiency and achievable bandwidth of modern communication devices. Here, we demonstrate that the introduction of metallic point-defects (Ti, Zr, Hf) improves the piezoelectric modulus of as-received, unstrained, epitaxially grown AlN. The metals are incorporated by ion implantation with an acceleration energy of 30 keV to a fluence of 10^{15} at cm^{-2}, which causes an elongation along the wurtzite *c-axis*. The stored internal strain energy increases the piezoelectric polarization of the thin AlN layer. This can equivalently be described by an enhancement of the piezoelectric modulus d_{33}. The incorporation of 0.1 at. % Ti enhances the piezoelectric modulus by ~30%; significantly exceeding gains obtained by alloying with the same amount of Sc.

Published under license by AIP Publishing. https://doi.org/10.1063/5.0031047

Aluminum nitride (AlN) is a semiconducting, high temperature ceramic. In its single crystal form, it has unique properties such as high thermal conductivity,[1] large bandgap,[2] and low thermal drift.[1] Furthermore, AlN has the largest piezoelectric coefficient of the binary tetragonally bonded semiconductors showing piezoelectric coefficients e_{33} and e_{31} of 1.5 C m^{-2} and -0.59 C m^{-2}, respectively.[1,3] In addition, the material can be easily introduced into a device due to the compatibility with complementary metal–oxide–semiconductor (CMOS) technology. Together, these properties led to the introduction of AlN in various devices such as light emitting diodes (LED),[4] high frequency and high power transistors,[5–8] and acoustic wave resonators.[9–12] For a wide variety of applications, the piezoelectric coefficients e_{33} and e_{31} define the figure of merit of these devices. For wurtzite structures, it has been shown that alloying with rare-earths can yield significantly enhanced piezoelectric coefficients.[13–15] However, the low-abundance of rare-earth materials makes them expensive and, hence, they are undesirable for mass production. For this reason, alloying with more abundant materials such as MgHf, ZrNb, and MgZr has been proposed as an alternative. These effectively act as effective trivalent cations in the AlN structure.[16] Here, we demonstrate an alternative approach to improve the piezoelectric coefficient by strain engineering using ion beam implantation. Ion implantation was only mentioned previously as a potential way to achieve alloying via ion beam-doping without consideration of its potential to introduce strain.[17] Here, we demonstrate that alloying with trivalent ions is not required if strain is used to enhance the piezoelectric polarization of the material.

AlN crystallizes in the wurtzite structure with a C_{6v} point group.[1] It has high spontaneous polarization and high piezoelectric coefficients among the III-nitride semiconductors. The piezoelectric polarization along the *c-axis* and the crystal structure can be correlated by the piezoelectric coefficients according to $P_3 = e_{33}\,\varepsilon_3 + e_{31}\,(\varepsilon_1 + \varepsilon_2)$[1,3] with the strain expressed in dependence of the *a*-axis and *c*-axis wurtzite unit cell parameters according to $\varepsilon_3 = (c - c_0)/c_0$ and $\varepsilon_1 = \varepsilon_2 = (a-a_0)/a_0$. The parameters a_0 and c_0 refer to the unstrained lattice constants for AlN and are 0.31 113 nm and 0.498 079 nm, respectively.[18] By definition, the piezoelectric coefficients are related to the piezoelectric moduli

Published under license by AIP Publishing

d_{xy} through a stress–strain relation.[13,14] For linear elastic properties, this is described by the elastic stiffness tensor. In the absence of shear stress, the piezoelectric polarization can be described by $P_3 = e_{33}\,\varepsilon_3 + e_{31}\,(\varepsilon_1 + \varepsilon_2) = d_{33}\,\sigma_3 + d_{31}\,(\sigma_1 + \sigma_2)$.[19] The total polarization P_{Total} along the *c-axis* is the sum of the piezoelectric polarization and the spontaneous polarization P_{SP}.

In this investigation, we use ion implantation to tune the strain of wurtzite AlN and demonstrate an increase in the piezoelectric coefficient and piezoelectric moduli after ion implantation. We compare two different samples grown by plasma vapor deposition (sample A) and molecular-beam epitaxy (sample B). Both samples have a 100 nm AlN film on Si (111) with the wurtzite *c-axis* aligned perpendicular to the Si surface. As we will show below, these samples provide different starting strain conditions. The samples with dimensions of $1 \times 1\,\text{cm}^2$ have been implanted with divalent metals (Ti, Zr, Hf). The fluence of 10^{15} at.cm^{-2} ensures negligible damage to the AlN crystal during ion implantation.[20–22] For all implantations, an acceleration energy of 30 keV has been used and a homogeneous distribution on the sample in the in-plane axis is achieved by scanning the ion beam over the implanted area. Details of the implantation setup and residual gas pressures are described elsewhere.[23,24]

The macrostrain of the wurtzite has been determined by x-ray diffraction (XRD) performed on a Rigaku SmartLab diffractometer using the Co K_α line ($\lambda = 0.179026$ nm). Both macroscopic strains are determined in two different geometries using an in-plane configuration for the AlN $\langle 100 \rangle$ band to determine ε_1 and out-of-plane geometry for the AlN $\langle 002 \rangle$ band to determine ε_3. Figure 1 shows the diffractograms before and after ion implantation.

Figure 1 reveals that both samples are subject to biaxial strain along the substrate's axis in comparison to the unstrained AlN wurtzite indicated by the dashed line. However, the strain of the as-received sample A is smaller in comparison to sample B. After ion implantation, a tensile strain along the *c-axis* emerges for both substrates [Fig. 1(a)]. For the wurtzite *a-axis*, no significant changes are observed due to metal ion implantation at the investigated fluence. Reciprocal space maps (RSM) of sample A on the symmetric AlN $\langle 002 \rangle$ band before and after 10^{15} at.cm^{-2} Ti have been obtained (supplementary material S1) and confirm subsequent strain interpretation, which is discussed later. In addition, we measured the rocking curves of the AlN $\langle 002 \rangle$ band, which have a full-width-half-maximum (FWHM) of 2.4° for sample A and 0.6° for sample B, before and after ion implantation (not shown).

From the XRD diffractograms, we extract the piezoelectric polarization from the average macroscopic strain, according to Eq. (1),

$$P_3 = 2e_{31} \int_{35}^{40} \varepsilon_1(2\theta) I_{\langle 100 \rangle}(2\theta)\, d(2\theta) + e_{33} \int_{40}^{44} \varepsilon_3(2\theta) I_{\langle 002 \rangle}(2\theta)\, d(2\theta). \tag{1}$$

The magnitude of the integral in the first and second terms is shown in Fig. 2, in conjunction with the relevant total polarization along the *c-axis*.

Figure 2 shows only a small deviation of ε_1 after ion implantation for all samples. This is in good agreement with observations on GaN demonstrating that the wurtzite *a-axis* is more resilient to ion radiation damage than the c-axis.[25] Only the as-received sample A shows

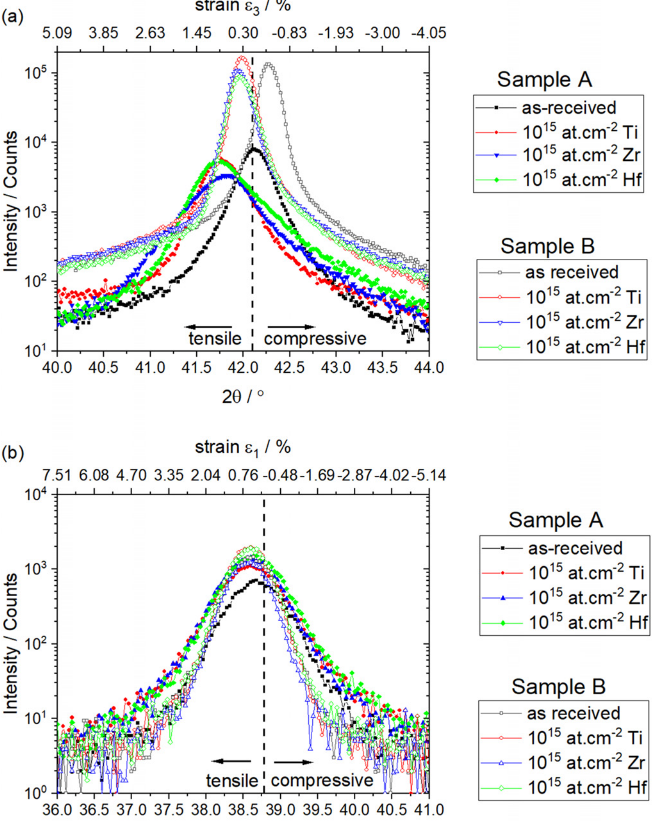

FIG. 1. XRD diffractograms of (a) $\langle 002 \rangle$ AlN and strain ε_3 in out-of-plane geometry and (b) $\langle 100 \rangle$ AlN and strain ε_1 in in-plane geometry. In both cases, the vertical dashed line represents the position for unstrained wurtzite AlN.[18]

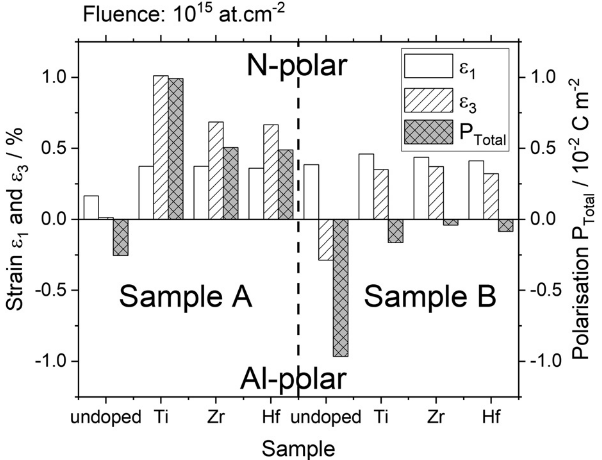

FIG. 2. Extracted average strain along the *a-axis* ε_1 and *c-axis* ε_3 and the calculated total polarization along the AlN *c-axis*.

Published under license by AIP Publishing

reduced strain along the *a-axis*. In contrast, the strain ε_3 varies significantly for different ion implantation conditions. Notably, the as-received sample B shows a significant compressive strain $\varepsilon_{3,}$ while only a small strain is present for sample A. Under the investigated conditions, ion implantation causes a tensile strain $\varepsilon_{3,}$ which is most significant for Ti implantation on sample A. We attribute the lower tensile strain after ion implantation in sample B to a compensation of the compressive strain in the as-received AlN.

Based on the derived strains, the total polarization is calculated and shown in Fig. 2. It shows that for sample B, the magnitude of polarization reduces, which, in turn, is expected to reduce the piezoelectric modulus. Hence, no improvement of the electromechanical response after ion implantation is anticipated. In contrast, the relaxed AlN (sample A) shows an increase in the polarization magnitude after ion implantation and a change of the polarization orientation. Thus, ion implantation effectively induces internal strain into the piezoelectric material, which can be used to increase the piezoelectric polarization and thus the piezoelectric modulus d_{33}.

These results strongly suggest that an increase in the amplitude of the piezoelectric polarization is only achievable if the AlN film is in a low-stress state as is present in sample A. In contrast, the calculations of polarization for undoped sample B reveal a large piezoelectric polarization due to the presence of large biaxial stress, which counteracts the benefits of ion implantation. Thus, from the XRD spectra, an improvement of the piezoelectric moduli is only expected for sample A, while a reduction is expected for sample B.

Evaluation of the piezoelectric moduli d_{33} is performed using Piezo Force Microscopy (PFM) on a NanoSurf FlexAFM. A PtSi-NCH tip with a typical radius of curvature of 25 nm. The tip has a cantilever force constant of 30 N/m, which ensures a low force of electrostatic interactions.[26] A tip force of 500 nN was applied to the surface. Measurements were performed with an alternating voltage between 2 V and 10 V with a frequency of 1 kHz, and the electromechanical response of the sample was recorded by measuring the amplitude (h) of the normal deflection of the tip with the lock-in amplifier. The effective piezoelectric modulus d_{33}^{eff} is obtained from the slope of the deflection amplitude at different voltages according to $h \approx d_{33}^{eff} V_{AC}$.

Figure 3 shows the results of the PFM data. In Fig. 3, the change of d_{33} after ion implantation for both samples are shown. For the as-received samples, we measured a d_{33} of 4.7 ± 0.3 pm V^{-1} and 6.1 ± 1.2 pm V^{-1} for samples A and B, respectively. Due to the large initial strains in sample B, the Si–AlN interface degrades and, thus, despite the high initial piezoelectric modulus, is not suitable for applications.

In good agreement with the calculated polarization in Fig. 2, sample A shows a significant increase in d_{33} for all three implantations. The largest increase is observed for the sample with maximum strain induced by Ti ion implantation. In contrast, all implantations into sample B show a relative decrease in the piezoelectric modulus. Thus, the calculated polarization based on the strain induced by ion implantation is in good qualitative agreement with the measured d_{33} by PFM.

In the following, we present a qualitative model explaining these results. The model is based on a set of assumptions supported by the literature: (a) the stress–strain relation is based on the mechanical constants of AlN (supplementary material S2) and deviations from the unstrained lattice can be described by biaxial, uniaxial, and hydrostatic strain.[27] (b) Defects in the crystal structure introduce a characteristic strain type, specifically: (b1) biaxial strain is caused by lattice mismatch to the substrate;[18,28–30] (b2) hydrostatic strain is caused by intrinsic defects;[18,31,32] and (b3) uniaxial strain is caused by the extrinsic defects Ti, Zr, and Hf. (c) The Hecking model describes the defects introduced by ion implantation.[20,21,33–35]

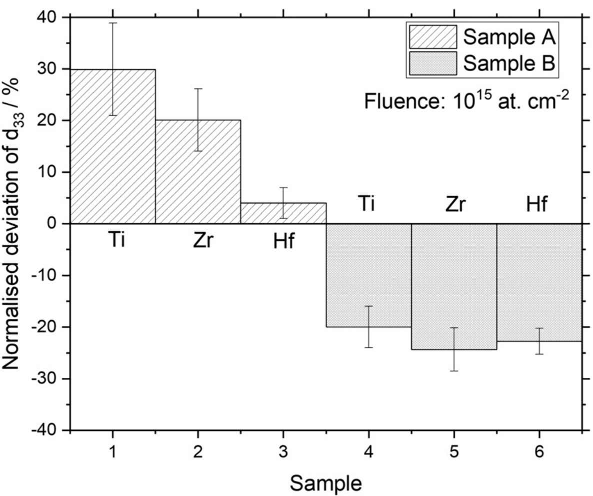

FIG. 3. Deviation of the piezoelectric modulus obtained by PFM in comparison to as-received AlN for both samples.

This model can be used to identify suitable ion implantation conditions to achieve better piezoelectric properties knowing the initial strain/stress condition of the AlN film. The qualitative results of our considerations are schematically shown in Fig. 4. Subsequently, we discuss the experimental evidence supporting the presented model.

Figure 4 illustrates that on both samples, the largest change in piezoelectric polarization is expected after Ti implantation. However, an improvement of the piezoelectric modulus is only obtained on sample A due to the high level of substrate-induced biaxial stress in the

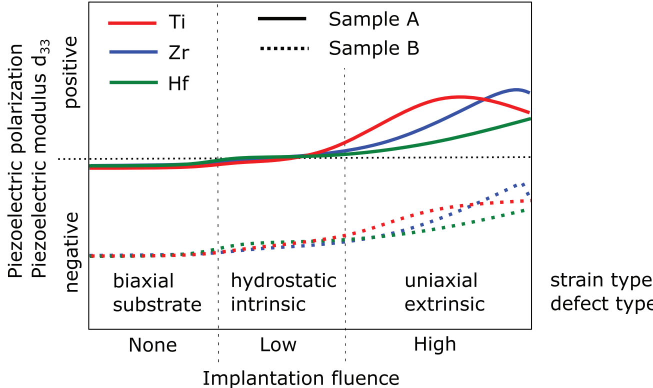

FIG. 4. Schematic illustration of the influence of ion implantation on the piezoelectric modulus d_{33}. This is dependent on the implanted ion type, implantation fluence, and substrate-induced biaxial strain (which dominates in sample B). The illustration separates the influence of hydrostatic strain caused by intrinsic defects at low fluences ($<10^{14}$ at cm^{-2}) and uniaxial strain caused by extrinsic defects at higher fluences ($>10^{14}$ at cm^{-2}).

Published under license by AIP Publishing

as-received sample B. Both samples A and B have a large interfacial energy at the Si–AlN interface. However, scanning transmission electron microscopy (STEM) of sample A revealed that biaxial strain is transferred to the Si substrate as shown by diffraction contrast and an absence of Moiré fringes in the near-interface region of the Si (supplementary material S6). This is in contrast to sample B where the biaxial strain is transferred to the AlN film, which leads to nucleation islands and subsequent amorphization of the crystalline Si at the interface.[11,22,36]

Subsequently, it is necessary to understand the physical origin of the emerging strains due to ion implantation. This is done using the established Hecking model that describes the changes in the number of point defects n_{pd} with the fluence N_I.[33] This model has been applied to describe radiative damage on a wide range of semiconductors, including $Al_xGa_{x-1}N$.[20,21,34,35] Since AlN is not prone to amorphization, two coupled differential equations determine the formation of point defects, according to Eq. (2),

$$\frac{dn_{np}}{dN_I} = P_{pd}e^{-R_{pd}N_I} + Cn_{pd}\left(1 - \frac{n_{pd}}{n^*_{pd}}\right). \qquad (2)$$

The first term describes the formation P_{pd} and recombination R_{pd} of intrinsic point defects, while the second term quantifies the formation of non-recombinable clusters of point defects with a kinetic parameter C and the saturation defect density of n^*. We further correlate the density of non-recombinable clusters with the implanted extrinsic defects.

The depth distribution of intrinsic and extrinsic defects has been simulated with the Monte Carlo program T-Dyn (supplementary material S3).[37] Those simulations enable the separation of five regions, which are directly overlayed with STEM images taken after implantation of 10^{15} at.cm^{-2} Ti^+ in Fig. 5(a).

This is consistent with the expected defects from the ion beam. According to the simulations, intrinsic defects are dominantly close to the surface, which introduces hydrostatic strain (Region A). Indeed, the shift of the 100 reflection along the *c-axis* in the diffractogram [inset; Fig. 5(c)] confirms this assignment. In contrast, the region B (16–30 nm) is dominated by extrinsic defects [Fig. 5(b)]; the visible distortions in the bright-field image make the reflections in the diffractogram more diffuse. The simulations also indicate that the region C 30–50 nm below the surface contains intrinsic and extrinsic defects, while in region D (50–67 nm), a low number of intrinsic defects is present. The region below (Region E) is not influenced by ion implantation and is shown in Fig. 5(d). Due to the proximity of the Si interface, biaxial strain dominates this region and the 002 reflections in the diffractogram Fig. 5(d) are split, accompanied by a broadening of all reflections, characteristic for biaxial strain.

For AlN, the recombination of intrinsic point defects is high and hence saturates for a low level of displacements per atoms. We attribute homogeneous tensile strain to intrinsic defects, thus contributing to a small positive change of piezoelectric polarization. According to Faye *et al.*, the defect saturation of AlN is reached for 0.022 vacancies cm^{-2}.[21] Monte Carlo simulations described in the supplementary material (S3) show that this concentration is exceeded for a significant proportion of the AlN film, even exceeding the range of the implanted metal. This interpretation is supported by the similar level of ε_1 after ion implantation irrespective of the implanted element and obtained RSM for 10^{15} Ti at cm^{-2} (supplementary material S1).

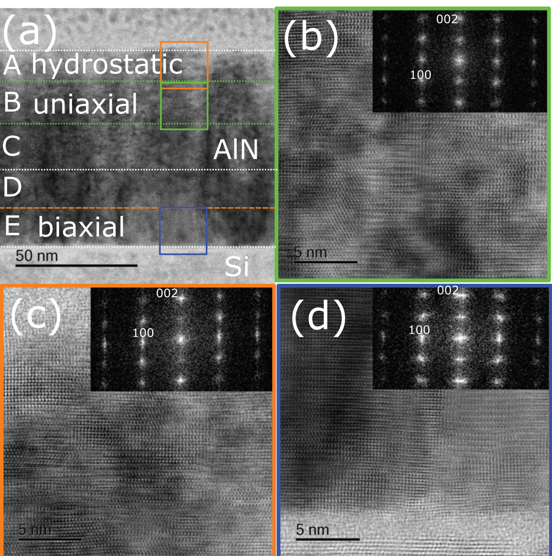

FIG. 5. Bright-field STEM images of sample A implanted with 10^{15} at cm^{-2} Ti^+. (a) Overview of the AlN film with the Si substrate at the bottom. The AlN layer is divided into five regions A–E, which, according to Monte Carlo simulations, are dominated by intrinsic defects (region A); Ti (region B); a low concentration of extrinsic and intrinsic defects (region C); a low concentration of intrinsic defects (region D); and beyond the implantation range (region E). The regions A, B, and E are dominated by one strain type and have been imaged with higher magnification (b)–(d) with the insets showing the respective diffractograms. (b) Region B is dominated by the uniaxial strain due to Ti. (c) Region A is dominated by hydrostatic defects due to intrinsic effects. (d) Region E is dominated by the biaxial strain due to the proximity to the substrate.

The formation of non-recombinable clusters is supported by the presence of external defects and thus directly depends on the concentration of the implanted element. The observed differences in the effectiveness of the different implantations (Ti > Zr > Hf) correspond to the reduced affected film volume with increasing mass of the implanted ion (supplementary material S3). Ti implantation affects 50% of the AlN film and a maximum Ti concentration of 6.0×10^{-3} at. nm^{-1} Ti is obtained. Zr and Hf only affect 33% and 20% of the film with maximum concentrations of 8.9×10^{-3} at. nm^{-1} and 12.6×10^{-3} at. nm^{-1}, respectively.

In the present case, we hypothesize that the lattice mismatch between the wurtzite AlN and a hypothetical stable rock salt nitride (XN; X = Ti, Zr, Hf) lattice defines the overall strain state. Since the w-AlN $(2\bar{1}0)$ plane and the rock salt nitride $(0\bar{1}1)$ plane are parallel with a lattice mismatch of less than 4%, a negligible strain is expected along the wurtzite *a-axis,* as experimentally confirmed in Fig. 1(b).[38] In contrast, the large lattice mismatch of >33% along the wurtzite c-axis leads to the observed uniaxial strain.

Calculating the number of overlapping lattice locations from the crystal lattice can then be used to estimate the number of Al atoms that can be substituted by the implanted metal without destabilizing the wurtzite crystal. Along each wurtzite *a-axis*, every fourth Al can be substituted, which is determined by the rotation of the unit cell while neglecting lattice mismatch. In contrast, along the *c-axis,* the wurtzite [002] and rock salt [001] axes are parallel, and the stable configuration is determined by the lattice mismatch. The lattice mismatches of 40%

Published under license by AIP Publishing

for Ti, 34% for Zr, and 35% for Hf provide an Al substitution factor of 5 for Ti and 3 for Zr and Hf. The maximum strain along the c-axis is thus expected for a concentration of 6.3×10^{-3} at. nm^{-1} Ti and 10.4×10^{-3} at. nm^{-1} for Zr and Hf. Since the unit cell of AlN contains two Al atoms, a translation vector between those two Al leads directly to a second rock salt lattice. Thus, a second stable configuration is achieved with the metal concentrations doubled.

Our experiments are in good agreement with estimations based on such symmetry considerations. Indeed, while the maximal uniaxial strain for Ti implantation is expected at 10^{15} at cm^{-2}, higher concentrations of Zr are required to achieve the same level of uniaxial strain, as Zr implantation affects a smaller volume. To verify this, we implanted AlN with Ti and Zr to a higher fluence of 10^{16} at cm^{-2}. The strain only increased in the case of Zr implantation (it decreased with Ti implantation), confirming this interpretation (supplementary material S4). In the case of Hf implantation into AlN, the implanted Hf rapidly exceeds the highest stable concentration even though the measured ε_3 strain is comparable to that of the Zr implantation. This results in a relatively smaller improvement of d_{33} observed after Hf implantation. This difference is likely due to larger strain after Hf implantation causing localized plastic deformations, which are not accounted for within this model.

The reported values for the piezoelectric modulus of AlN vary widely in the range of 3.0–7.0 pm.[11,39–42] Most of those values were obtained from thin AlN grown on silicon, which is a substrate known to introduce significant biaxial stress.[28,43,44] The absence of investigated bulk materials and the limited characterization of the stress state of AlN in those investigations are notable. In particular, the lowest reported piezoelectric coefficients are for films grown on SiC and Si(100) substrates.[39,41] Both substrates induce a low biaxial strain during growth because of the small mismatch between the SiC and AlN lattices. In the case of Si(100), the lattice mismatch is sufficiently large to inhibit epitaxial growth.[1,18,43] Our results suggest that the variations in earlier reported piezoelectric moduli can be attributed to different states of piezoelectric polarization induced by the biaxial stress from the substrate. There is no experimental report using the biaxial stress in AlN to modify the piezoelectric modulus reported in the literature. However, two recent reports on different materials support our interpretation: (1) stretching ZnO nanorods increases the piezoelectric coefficient[45] and (2) *in situ* XRD on Lead Zirconium Titanate confirms the direct correlation between piezoelectric polarization and the crystallography.[46]

A known method to increase the piezoelectric modulus is alloying with trivalent rare-earth metals or effective trivalent clusters.[13,16] These strategies destabilize AlN, which enhances the piezoelectric and spontaneous polarization.[19,47,48] Our implantation of Ti into AlN results in a maximum atomic fraction of 0.6 at. % and a total proportion of only 0.1 at. % of Ti in the AlN layer. This gives rise to an ~30% (6.1 pm V^{-1}) increase in the piezoelectric modulus. Based on the calculations by Caro *et al.* ($d_{33,AlN} = 5.1$ pm V^{-1}),[19] homogeneously alloying with Sc with the same amount of material would only yield an 8% (5.5 pm V^{-1}) increase in d_{33} with respect to the maximum atomic fraction or an increase in less than 1% (5.2 pm V^{-1}) with respect to the total amount of material. This contrasts to a 500% d_{33} (24.2 pm V^{-1};[15] 27.6 pm V^{-1}[13]) increase for an Sc concentration of 43 at. %,[13,15] not attainable by ion implantation due to excessive damage that it would incur. Thus, alloying is not responsible for the increase in the piezoelectric coefficient, whereas our increased piezoelectric coefficient originates from ion implantation-induced strain. Initial reports on ScN discussed the presence of the rock salt ScN—wurtzite AlN phase transformation; hence, we also applied our crystallographic strain considerations to ScN.[13] For $Sc_xAl_{x-1}N$, the strain would be minimized for $x = 0.33$ along the *c-axis*. For these conditions, the texture and piezoelectric coefficient depend strongly on the preparation conditions.[13–15]

In conclusion, we have demonstrated that ion implantation enables the strain in a relaxed, unstrained wurtzite piezoelectric, such as AlN, to be tuned to increase the piezoelectric modulus. In comparison to other methods, an increase in the piezoelectric modulus is achieved with a significant lower amount of alloying addition (by implantation). Furthermore, the described strain engineering by ion implantation can be applied after the deposition of the piezoelectric layer, something that is not feasible for other technologies. In addition, ion implantation could be combined with the rare-earth alloying approach to further enhance the piezoelectric coefficient of those materials. This technology has the potential to lead to devices with increased energy efficiency in acoustic wave filters with a reduced bandwidth, increased operation frequency, and reduced energy losses.

See the supplementary material for additional discussion of XRD, mechanical parameters, ion beam simulation, STEM analysis, PFM, and the effect of higher fluences.

The research was financed by the New Zealand Ministry for Business, Innovation, and Employment (No. C05X1712). This work used the JEOL JEM-ARM200F and FEI NanoLab G3 CX both funded by the Australian Research Council (ARC)—Linkage, Infrastructure, Equipment and Facilities (LIEF) Grant (Nos. LE120100104 and LE160100063, respectively) and located at the University of Wollongong Electron Microscopy Centre (UoW EMC), Australia. The authors wish to thank Dr. Mitchell Nancarrow (UoW EMC) for FIB specimen preparation.

DATA AVAILABILITY

The data that support the findings of this study are available from the corresponding author upon reasonable request.

REFERENCES

[1] O. Ambacher, "Growth and applications of group III-nitrides," J. Phys. D: Appl. Phys. **31**(20), 2653–2710 (1998).
[2] I. Vurgaftman and J. R. Meyer, "Band parameters for nitrogen-containing semiconductors," J. Appl. Phys. **94**(6), 3675–3696 (2003).
[3] F. Bernardini, V. Fiorentini, and D. Vanderbilt, "Spontaneous polarization and piezoelectric constants of III-V nitrides," Phys. Rev. B **56**(16), R10024–R10027 (1997).
[4] Y. Taniyasu, M. Kasu, and T. Makimoto, "An aluminium nitride light-emitting diode with a wavelength of 210 nanometres," Nature **441**(7091), 325–328 (2006).
[5] L. F. Eastman, V. Tilak, J. Smart, B. M. Green, E. M. Chumbes, R. Dimitrov, H. Kim, O. S. Ambacher, N. Weimann, T. Prunty, M. Murphy, W. J. Schaff, and J. R. Shealy, "Undoped AlGaN/GaN HEMTs for microwave power amplification," IEEE Trans. Electron Devices **48**(3), 479–485 (2001).
[6] B. E. Foutz, S. K. O'Leary, M. S. Shur, and L. F. Eastman, "Transient electron transport in wurtzite GaN, InN, and AlN," J. Appl. Phys. **85**(11), 7727–7734 (1999).
[7] S. Arulkumaran, G. I. Ng, Z. H. Liu, and C. H. Lee, "High temperature power performance of AlGaNGaN high-electron-mobility transistors on high-resistivity silicon," Appl. Phys. Lett. **91**(8), 083516 (2007).

Published under license by AIP Publishing

[8] S. Arulkumaran, G. I. Ng, S. Vicknesh, H. Wang, K. S. Ang, J. P. Y. Tan, V. K. Lin, S. Todd, G. Q. Lo, and S. Tripathy, "Direct current and microwave characteristics of sub-micron AlGaN/GaN high-electron-mobility transistors on 8-inch Si(111) substrate," Jpn. J. Appl. Phys., Part 1 **51**, 111001 (2012).

[9] G. Chen, X. Zhao, X. Wang, H. Jin, S. Li, S. Dong, A. J. Flewitt, W. I. Milne, and J. K. Luo, "Film bulk acoustic resonators integrated on arbitrary substrates using a polymer support layer," Sci. Rep. **5**, 9510 (2015).

[10] S. Tadigadapa and K. Mateti, "Piezoelectric MEMS sensors: State-of-the-art and perspectives," Meas. Sci. Technol. **20**(9), 092001 (2009).

[11] K. Tonisch, V. Cimalla, C. Foerster, H. Romanus, O. Ambacher, and D. Dontsov, "Piezoelectric properties of polycrystalline AlN thin films for MEMS application," Sens. Actuators, A **132**(2), 658–663 (2006).

[12] J. Wang, M. Park, S. Mertin, T. Pensala, F. Ayazi, and A. Ansari, "A film bulk acoustic resonator based on ferroelectric aluminum scandium nitride Films," J. Microelectromech. Syst. **29**(5), 741–747 (2020).

[13] M. Akiyama, T. Kamohara, K. Kano, A. Teshigahara, Y. Takeuchi, and N. Kawahara, "Enhancement of piezoelectric response in scandium aluminum nitride alloy thin films prepared by dual reactive cosputtering," Adv. Mater. **21**(5), 593–596 (2009).

[14] A. Zukauskaite, G. Wingqvist, J. Palisaitis, J. Jensen, P. O. A. Persson, R. Matloub, P. Muralt, Y. Kim, J. Birch, and L. Hultman, "Microstructure and dielectric properties of piezoelectric magnetron sputtered w-$Sc_xAl_{1-x}N$ thin films," J. Appl. Phys. **111**(9), 093527 (2012).

[15] M. Akiyama, K. Kano, and A. Teshigahara, "Influence of growth temperature and scandium concentration on piezoelectric response of scandium aluminum nitride alloy thin films," Appl. Phys. Lett. **95**(16), 162107 (2009).

[16] T. Yokoyama, Y. Iwazaki, Y. Onda, T. Nishihara, Y. Sasajima, and M. Ueda, "Highly piezoelectric co-doped AlN thin films for wideband FBAR applications," IEEE Trans. Ultrason., Ferroelectr., Freq. Control **62**(6), 1007–1015 (2015).

[17] M. Akiyama, T. K. N. Ueno, K. Kano, A. Teshigahara, Y. Takeuchi, and N. Kawahara, "Piezoelectric thin film, piezoelectric material, and fabrication method of piezoelectric thin film and piezoelectric material, and piezoelectric resonator, actuator element, and physical sensor using piezoelectric thin film," U.S. patent 7,758,979 B2 (2010).

[18] D. Nilsson, E. Janzén, and A. Kakanakova-Georgieva, "Lattice parameters of AlN bulk, homoepitaxial and heteroepitaxial material," J. Phys. D: Appl. Phys. **49**(17), 175108 (2016).

[19] M. A. Caro, S. Zhang, T. Riekkinen, M. Ylilammi, M. A. Moram, O. Lopez-Acevedo, J. Molarius, and T. Laurila, "Piezoelectric coefficients and spontaneous polarization of ScAlN," J. Phys. Condens. Matter **27**(24), 245901 (2015).

[20] D. N. Faye, M. Döbeli, E. Wendler, F. Brunner, M. Weyers, S. Magalhães, E. Alves, and K. Lorenz, "Crystal damage analysis of implanted $Al_xGa_{1-x}N$ ($0 \le x \le 1$) by ion beam techniques," Surf. Coat. Technol. **355**, 55–60 (2018).

[21] D. N. Faye, E. Wendler, M. Felizardo, S. Magalhães, E. Alves, F. Brunner, M. Weyers, and K. Lorenz, "Mechanisms of implantation damage formation in $Al_xGa_{1-x}N$ compounds," J. Phys. Chem. C **120**(13), 7277–7283 (2016).

[22] H. Fiedler, V. Jovic, D. R. G. Mitchell, J. Leveneur, E. Anquillare, K. E. Smith, and J. Kennedy, "Tuning the electromechanical properties and polarization of aluminium nitride by ion beam-induced point defects," Acta Mater. **203**, 116495 (2021).

[23] H. Fiedler, P. Gupta, J. Kennedy, and A. Markwitz, "28 Si + ion beams from Penning ion source based implanter systems for near-surface isotopic purification of silicon," Rev. Sci. Instrum. **89**(12), 123305 (2018).

[24] A. Markwitz and J. Kennedy, "Group-IV and v ion implantation into nanomaterials and elemental analysis on the nanometre scale," Int. J. Nanotechnol. **6**(3–4), 369–383 (2009).

[25] K. Lorenz, E. Wendler, A. Redondo-Cubero, N. Catarino, M. P. Chauvat, S. Schwaiger, F. Scholz, E. Alves, and P. Ruterana, "Implantation damage formation in a-, c-, and m-plane GaN," Acta Mater. **123**, 177–187 (2017).

[26] S. Kim, D. Seol, X. Lu, M. Alexe, and Y. Kim, "Electrostatic-free piezoresponse force microscopy," Sci. Rep. **7**, 41657 (2017).

[27] J. M. Wagner and F. Bechstedt, "Properties of strained wurtzite GaN and AlN: Ab initio studies," Phys. Rev. B **66**(11), 15202 (2002).

[28] V. Lughi and D. R. Clarke, "Defect and stress characterization of AlN films by Raman spectroscopy," Appl. Phys. Lett. **89**(24), 241911 (2006).

[29] K. Shojiki, Y. Hayashi, K. Uesugi, and H. Miyake, "Local and anisotropic strain in AlN film on sapphire observed by Raman scattering spectroscopy," Jpn. J. Appl. Phys., Part 1 **58**(SC), SCCB17 (2019).

[30] S. Yang, R. Miyagawa, H. Miyake, K. Hiramatsu, and H. Harima, "Raman scattering spectroscopy of residual stresses in epitaxial AlN films," Appl. Phys. Express **4**(3), 031001 (2011).

[31] C. Kisielowski, J. Krüger, S. Ruvimov, T. Suski, J. Ager, E. Jones, Z. Liliental-Weber, M. Rubin, E. Weber, M. Bremser, and R. Davis, "Strain-related phenomena in GaN thin films," Phys. Rev. B **54**(24), 17745–17753 (1996).

[32] T. Pornphatdetaudom, K. Yoshida, and T. Yano, "Recovery behavior of neutron-irradiated aluminum nitride with and without containing interstitial dislocation loops," J. Nucl. Mater. **543**, 152584 (2021).

[33] N. Hecking, K. F. Heidemann, and E. Te Kaat, "Model of temperature dependent defect interaction and amorphization in crystalline silicon during ion irradiation," Nucl. Instrum. Methods Phys. Res., Sect. B **15**(1–6), 760–764 (1986).

[34] E. Wendler, "Mechanisms of damage formation in semiconductors," Nucl. Instrum. Methods Phys. Res., Sect. B **267**(16), 2680–2689 (2009).

[35] E. Wendler and W. Wesch, "Ar implantation of InSb and AlN at 15 K," Nucl. Instrum. Methods Phys. Res., Sect. B **242**(1–2), 562–564 (2006).

[36] N. Mante, S. Rennesson, E. Frayssinet, L. Largeau, F. Semond, J. L. Rouvière, G. Feuillet, and P. Vennéguès, "Proposition of a model elucidating the AlN-on-Si (111) microstructure," J. Appl. Phys. **123**(21), 215701 (2018).

[37] W. Möller and W. Eckstein, "Tridyn—A TRIM simulation code including dynamic composition changes," Nucl. Instrum. Methods Phys. Res., Sect. B **2**(1–3), 814–818 (1984).

[38] B. Saha, S. Saber, E. A. Stach, E. P. Kvam, and T. D. Sands, "Understanding the rocksalt-to-wurtzite phase transformation through microstructural analysis of (Al,Sc)N epitaxial thin films," Appl. Phys. Lett. **109**(17), 172102 (2016).

[39] I. L. Guy, S. Muensit, and E. M. Goldys, "Extensional piezoelectric coefficients of gallium nitride and aluminum nitride," Appl. Phys. Lett. **75**(26), 4133–4135 (1999).

[40] C. M. Lueng, H. L. W. Chan, C. Surya, and C. L. Choy, "Piezoelectric coefficient of aluminum nitride and gallium nitride," J. Appl. Phys. **88**(9), 5360–5363 (2000).

[41] B. J. Rodriguez, A. Gruverman, A. I. Kingon, and R. J. Nemanich, "Piezoresponse force microscopy for piezoelectric measurements of III-nitride materials," J. Cryst. Growth **246**(3–4), 252–258 (2002).

[42] F. Martin, P. Muralt, M. A. Dubois, and A. Pezous, "Thickness dependence of the properties of highly c-axis textured AIN thin films," J. Vac. Sci. Technol., A **22**(2), 361–365 (2004).

[43] X. Wang and A. Yoshikawa, "Molecular beam epitaxy growth of GaN, AlN and InN," Prog. Cryst. Growth Charact. Mater. **48–49**(1–3), 42–103 (2004).

[44] T. Prokofyeva, M. Seon, J. Vanbuskirk, M. Holtz, S. A. Nikishin, N. N. Faleev, H. Temkin, and S. Zollner, "Vibrational properties of AlN grown on (111)-oriented silicon," Phys. Rev. B **63**(12), 125313 (2001).

[45] H. J. Choi, Y. S. Jung, J. Han, and Y. S. Cho, "*In-situ* stretching strain-driven high piezoelectricity and enhanced electromechanical energy-harvesting performance of a ZnO nanorod-array structure," Nano Energy **72**, 104735 (2020).

[46] G. Tan, K. Maruyama, Y. Kanamitsu, S. Nishioka, T. Ozaki, T. Umegaki, H. Hida, and I. Kanno, "Crystallographic contributions to piezoelectric properties in PZT thin films," Sci. Rep. **9**(1), 7309 (2019).

[47] M. A. Caro, S. Schulz, and E. P. O'Reilly, "Theory of local electric polarization and its relation to internal strain: Impact on polarization potential and electronic properties of group-III nitrides," Phys. Rev. B **88**(21), 214103 (2013).

[48] F. Tasnádi, B. Alling, C. Höglund, G. Wingqvist, J. Birch, L. Hultman, and I. A. Abrikosov, "Origin of the anomalous piezoelectric response in wurtzite $Sc_xAl_{1-x}N$ alloys," Phys. Rev. Lett. **104**(13), 137601 (2010).

Published under license by AIP Publishing